Cardiovascular Magnetic Resonance in Mice

Ulrich Flögel, Experimental Cardiovascular Imaging Heinrich Heine University Düsseldorf, Germany floegel@uni-duesseldorf.de

Introduction

Today, magnetic resonance imaging (MRI) is undoubtedly the leading technique in diagnostic imaging. However, MRI techniques are not only crucial in the clinical setting, but are also of major importance for basic research to explore pathomechanisms and potential novel therapeutic targets in animal models of human diseases. Providing superior contrast between soft-tissues and due its multifaceted field of applications, MRI allows an accurate and longitudinal *in vivo* analysis also of cardiovascular relevant disease models[1–3]. Beyond morphology, magnetic resonance spectroscopy (MRS) can be exploited to address important metabolic processes[4–6], which are mandatory for the proper function of the heart. To study also dynamic processes in vascular biology, such as the development of vessel stenosis or the initiation of neovascularization magnetic resonance angiography (MRA) can additionally be employed[7,8]. Due to its non-invasive nature all techniques as well perfectly matches current requirements of animal care, such as the 3Rs (replacement, reduction and refinement), since over the entire period of investigation all data are obtained from the same individuals, thereby reducing the number of animals and increasing the reliability of the acquired results.

On the negative side, it was conventionally argued that MRI suffers from low sensitivity compared to other imaging modalities. However, a new generation of nanotechnology-based contrast agents is making it possible to overcome this limitation and bring MRI into the molecular imaging category. In this context, fluorine (^{19}F) MRI has lately garnered significant scientific interest in the biomedical research community[9], due to the unique properties of fluorinated materials and the ^{19}F nucleus. The stable fluorine isotope ^{19}F naturally occurs to 100% and exhibits an intrinsic sensitivity for MRI close to that of the ^{1}H nucleus[10], which is commonly used to produce detailed anatomical images. There is negligible endogenous ^{19}F in the body and, thus, no background signal which allows the detection of fluorinated materials as 'hotspots'[11] by combined ^{1}H/^{19}F MRI and renders fluorine-containing molecules as ideal tracers for a wide variety of MRI applications.

The most commonly used animal model in basic reseach is the mouse, which can easily be genetically modified to mimic inherited human gene defects or to explore specific signalling pathways as target for therapy. However, for murine MRI studies dedicated hardware is required to enable high resolution analysis of the small organs. In particular imaging of the mouse heart characterized by low mass and very high heart rates compared to human conditions (~0.1 vs 300 gram heart weight; 600 vs 60 beats per minute) is a very challenging task. Nevertheless, by choosing appropriate acquisition parameters and coil setups, images of excellent quality can also be obtained from this species as demonstrated below.

Experimental

General: Data are recorded at a Bruker AVANCEIII 9.4T wide bore NMR spectrometer driven by ParaVision 5.1 (Bruker, Rheinstetten, Germany) and operating at frequencies of 400.21 MHz for ^{1}H and 376.54 Mhz for ^{19}F measurements. Images are acquired using a Bruker microimaging unit Micro2.5

with actively shielded gradient sets (1.5 T/m) and a 25-mm ^{1}H quadrature resonator for cine loops, spectroscopy, and angiography or a 25-mm quadrature resonator tunable to ^{1}H (linear) and ^{19}F (quadrature) for inflammation imaging. Mice are anaesthetized with 1.5% isoflurane and kept at 37 °C. The front-paws and the left hind-paw are attached to ECG electrodes (Klear-Trace; CAS Medical Systems, Branford) and respiration is monitored by means of a pneumatic pillow positioned at the animal's back. Vital functions are acquired by a M1025 system (SA Instruments, Stony Brook, NY, USA) and used to synchronize data acquisition with cardiac and respiratory motion.

Figure 1

MicWB40 Mouse Heart Coil.

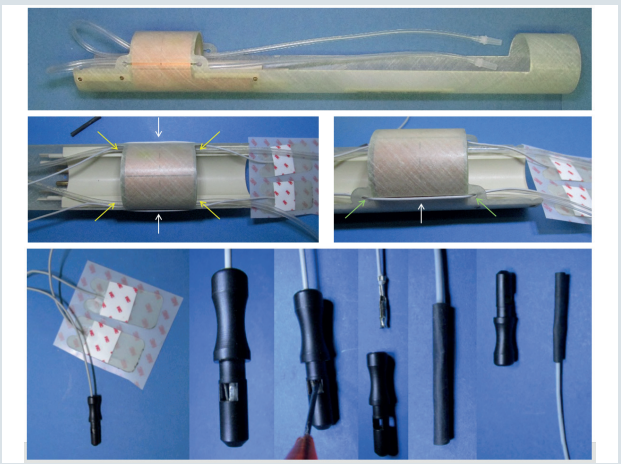

Figure 1: Design of the quad-resonator for cardiovascular applications.

Top: Overview over the RF insert. Middle: Increased views of the insert showing guidance of the electrode wires through the tiny grooves at the outside of the probe (white arrows) and passing of the anesthesia tubes through the wall of the resonator in between its coils (yellow arrows). Bottom: Modification of the standard ECG electrode connectors to fit the feeding to the grooves (green arrows middle right).

Since the wide bore spectrometers are usually installed without Faraday cage, the use of ECG electrodes inside the magnet is prone to cause antenna problems resulting in zipper artifacts and substantially reduced SNR in the MR images. This can be overcome by placing the leads of the electrodes around the resonator in tiny grooves at the outside of the probe (Figure 1). The subsequent fixing of the ECG electrodes for the front/hind-paws just before/behind the resonator as illustrated in Figure 2 avoids any radiofrequency interferences. Of note, passing the inlet/outlet tubes for the anesthesia gas through the wall of the resonator in between its coils (Figures 1+2) both improves the field homogeneity and saves some space for the object of interest within the sensitive volume.

For *functional and morphometric analysis*, high resolution images of mouse hearts are acquired in short axis orientation using an ECG- and respiratory-gated segmented fast gradient echo cine sequence with steady state precession (FISP)[12]. A

Figure 2

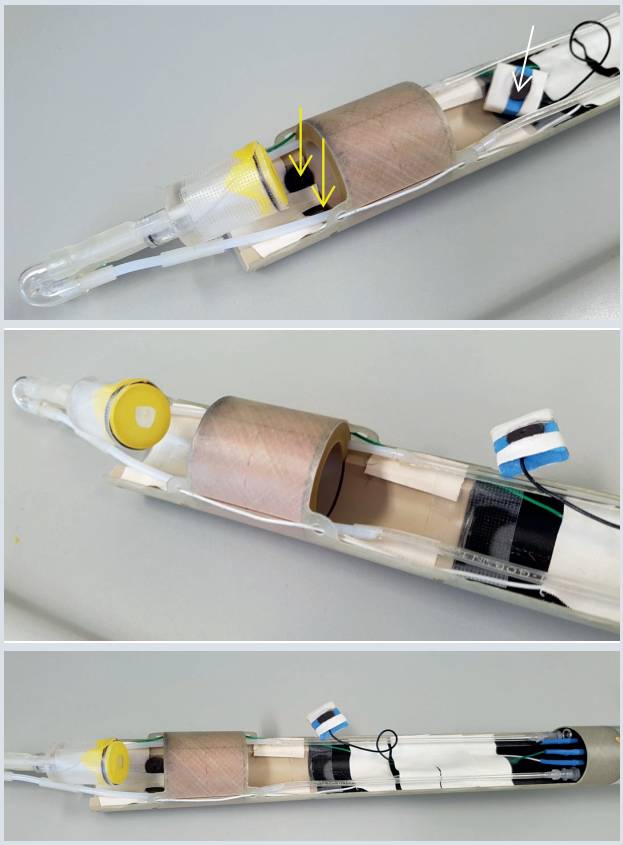

Figure 2: Resonator with anesthesia equipment mounted to the probe.

Different views of the RF insert with anesthesia mask (with inlet and outlet) as well as front- and hind-paw electrodes (top: yellow and white arrows, respectively) connected to the ECG adapters of the probe (bottom: blue pins).

flip angle (FA) of 15°, echo time (TE) of 1.23 ms, and a repetition time (TR) of about 6-8 ms (depending on the heart rate) are used to acquire 16 frames per heart cycle with an in plane resolution of 58.5×58.5 μm^2 after zerofilling (field of view (FOV), 30×30 mm^2; matrix, 256×256; slice thickness (ST), 1 mm; number of averages (NA), 3; acquisition time (TAcq) per slice for one cine loop, ~2.5 min). Routinely, 8-10 contiguous short axis slices are required for complete coverage of the LV, which is ensured by longitudinal slices orientated perpendicular to the atrio-ventricular level. For evaluation of functional parameters (e.g. EDV, ESV, EF), ventricular demarcations in end-diastole and -systole are manually drawn with the ParaVision Region-of-Interest (ROI) tool.

For localized ^{1}H MRS, a 1×2×3 mm^3 voxel is placed in the septum as described previously[13]. Fieldmap-based shimming (MAPSHIM) is carried out to optimize the field homogeneity in the region of interest followed by manual shimming. ^{1}H MR spectra are acquired using ECG- and respiratory-gated single-voxel point resolved spectroscopy (PRESS) with a chemical shift selective (CHESS) water suppression module and outer volume suppression (OVS). The following param-

eters are used: TR, 1000 ms; TE, 9.1 ms; averages, 1024; data points in the spectral domain, 256; spectral width, 5000 Hz; acquisition time, 51.2 ms; an exponential filter of 10 Hz is applied and chemical shifts are referenced to the prominent triglyceride methylene (-CH2-) peak in the water-suppressed spectra at 1.3 ppm. The exact repetition time of the sequence is determined by heart and respiration rates of the individual mice. Total preparation time including CHESS (73.23 ms) and OVS (18.63 ms) is 91.86 ms. Localized acquisition is timed at ~40% of the cardiac cycle in systole to maximize tissue thickness and homogeneity, typically requiring a trigger delay of 60 to 80 ms after ECG R-wave upslope detection. Water-suppressed and unsuppressed cardiac spectra from the same voxel positioned in the septum are acquired in using the PRESS sequence with and without CHESS suppression. To quantify the myocardial metabolite content, the integral of the lipid signal is divided by the corresponding integral of the water signal from unsuppressed spectra, thus reporting lipid content as a percentage of the water signal.

MR angiography is carried out essentially as described previously.[7,8,14] Collateral vessel formation is monitored using a flow-compensated 2D time-of-flight (TOF) fast low angle shot (FLASH) sequence 21 days after induction of hindlimb ischemia (flip ange 80°, echo time (TE) 2.52 ms; repetition time (TR) 10 ms, number of scans (NS) 3, acquisition time (TAcq) 20 minutes, in plane FOV 25.6×25.6 mm^2 with a spatial resolution of 50×50 μm^2 after zero filling). In z-direction the FOV is set to cover the entire vessel system from the bifurcation of the femoral artery down to the hind paws (210 overlapping slices with a slice thickness (ST) of 0.3 mm and an interslice distance of 0.18 mm resulting in a package extent of 37.92 mm). Subsequently, data are imported into the 3D visualization software Amira 4.0 (Mercury Computer Systems) and are resampled to isotropic voxel size using a Lanzcos filter. 3D data are visualized in maximum intensity projection using the Voltex module and application of the 'glow' look-up table of Amira. For quantification, an isosurface is calculated for the entire vessel system by applying a constant threshold to all data sets. Afterwards, the area of interest (here the newly formed collaterals) is separated from the remaining vessels using the VolumeEdit tool of Amira. Finally, the extracted surface is used to calculate the collateral vessel volume.

Inflammation imaging: For visualization of inflammatory processes, mice receive an intravenous bolus injection of a 10% perfluoro-15-crown-5 ether emulsion (PFC, 3 mM/kg BW) 48 h prior to MRI to ensure appropiate PFC-loading of circulating immune cells.[15] After acquisition of all ^{1}H datasets as described above, the resonator is tuned to ^{19}F, and morphologically matching ^{19}F images are recorded. For superimposing the images of both nuclei, the 'hot iron' color look-up table provided by ParaVision is applied to ^{19}F images. To fade out the background noise from ^{19}F images a constant threshold is applied to ^{19}F data. ^{19}F multislice rapid acquisition with relaxation enhancement (RARE) images are recorded from the same FOV as the functional data in short axis orientation (RARE factor 32, TR 2500 ms; TE 3.88 ms, MS 64x64, 8-10 slices, ST 1 mm, averages 256, TAcq 21.3 min). Inflamed regions are determined from ^{19}F images by planimetric analysis of PFC signals using the ROI tool of ParaVision. For a more detailed description of the ^{19}F MRI approach, acquisition parameters, and quantification procedures, please refer to references.[15,16] The full experimental protocol takes around 60-90 min and is well tolerated by all mice which recover from anesthesia within 1–2 min.

RESULTS

^{1}H MR for murine cardiovascular anatomy, function, and metabolism

Examples of high resolution end-diastolic MR images of the murine heart acquired with the setup described above are illustrated in Figure 3 top. Left top shows a healthy murine heart in long axis orientation with superb illustration of the left and right ventricle, the aortic valve as well as the aortic arch with passing of the two carotid and the left subclavian arteries. Furthermore, the pulmonary artery and both atria can clearly be recognized. In Figure 3 right top a short axis slice of a hypertrophied murine heart is displayed. Please note the massive trabeculation and thickening of the left ventricular wall as compared to the healthy heart on the left. In this mid-ventricular short axis view, also the papillary muscles are pretty well resolved. They attach to the atrioventricular valves and thereby prevent inversion of these valves on systole.

Figure 3 left bottom represents a volume-selective water-suppressed ^{1}H MR spectrum acquired from a spectroscopic voxel (6 µl) placed in the interventricular septum (rectangle in right top). Compared to the free ventricular wall, the septum is less affected by motion/displacement during the cardiac cycle. Data acquisition is carried out in end-systole to ensure highest muscle thickness and suspended coronary perfusion resulting in enhanced tissue homogeneity and improved shim. As can be seen, the major signals for creatine, taurine, choline, and lipids with discrimination of mono- and polyunsaturated fatty acids (FA) are well resolved and can easily be quantified to monitor dynamic metabolic changes during development of heart diseases[13,17].

Finally, in Figure 3 right bottom the vessel system of the murine hindlimbs is imaged by contrast agent free time-of-flight MR angiography revealing the evolution of collateral vessels to compensate for perfusion deficits in the periphery around the paws. The coronal MR angiogram is displayed as maximum intensity projection (MIP), showing in great detail the entire vessel tree with the femoral arteries and its branches into the popliteal artery. The image clearly shows the diminished perfusion of the left hind limb (yellow arrows) as well as origin, course, and re-entry zones of the newly developed collateral vessels (white arrows). Collaterals are characterized by their corkscrew morphology, typical for arteriogenesis, during which growth in length outpaces increase in diameter[18].

Figure 3

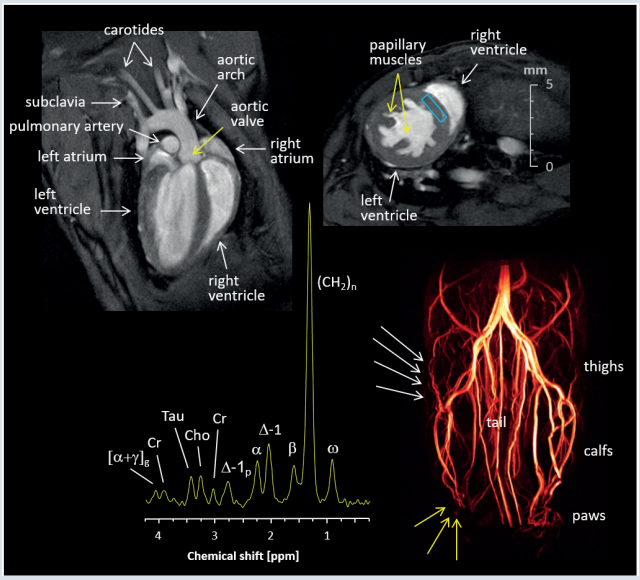

Figure 3: Cardiovascular applications of ^{1}H MRI and MRS.
Left top: Healthy murine heart in long axis orientation showing a plenty of anatomical details (see text). Right top: Short axis slice of a hypertrophied murine heart with massive trabeculation and thickening of the left ventricular wall as compared to the left. Left bottom: ^{1}H MR spectrum acquired from the rectangle in the interventricular septum (right top). Signal assignment: $[\alpha+\gamma]_g$, bound to α+γ carbons of the triglyceride's glycerol backbone; Cr, creatine; Tau, taurine; Cho, choline; $\Delta\text{-}1_p$, next to polyunsaturated fatty acids (FA) carbons; α, bound to the α-carbon of FA; Δ-1, next to monounsaturated FA carbons; β, bound to the β-carbon of FA; $(CH_2)_n$, methylene groups of FA; ω, terminal methyl group of FA. Right bottom: Vessel system of the murine hindlimbs revealing the evolution of collateral vessels (white arrows) to compensate for perfusion deficits in the periphery around the paws (yellow arrows).

^{19}F MR inflammation imaging

The recent application of ^{19}F MRI for molecular imaging takes advantage of the fact, that intravenously applied perfluorocarbon nanoemulsions (PFCs) are efficiently taken up by circulating cells of the innate immune system, in particular monocytes and macrophages[19]. The subsequent migration of the ^{19}F-loaded, immunocompetent cells into inflammatory foci then permits the unambiguous *in vivo* identification of affected regions by combination of ^{1}H and ^{19}F MRI. This is illustrated in a murine model of myocardial infarction[15] induced by occlusion of a coronary artery – a procedure well known to be associated with an acute inflammatory response in the affected tissue.

Figure 4 upper row demonstrates the principle of the combined ^{1}H/^{19}F MRI approach: The end-diastolic ^{1}H image (left) clearly shows the presence of ventricular dilatation and wall thinning within the infarcted area of the heart, and in the corresponding ^{19}F image (middle), the signal pattern matches the shape of the free left ventricular wall. For merging of the original gray scale images, a ‚hot iron' lookup table is applied to the fluorine data, which allows a convenient discrimination of the signals from the ^{1}H and ^{19}F nucleus. The resulting overlay (right) confirms the localization of PFCs within the anterior, lateral, and posterior walls. Furthermore, ^{19}F signal also is detected in the adjacent chest tissue, where thoracotomy for the surgical intervention was performed. Note that otherwise no background ^{19}F signal from other tissue is present.

Figure 4

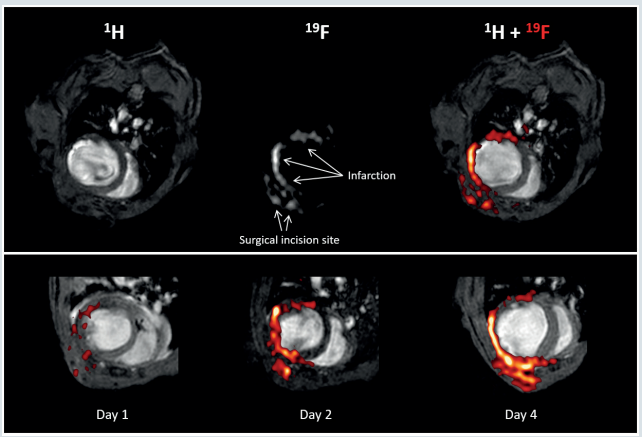

Figure 4: Visualization of inflammation after myocardial infarction by *in vivo* ^{19}F MRI.
Top: Anatomically corresponding ^{1}H (left) and ^{19}F (middle) images from the mouse thorax recorded 6 days after ligation of the left anterior descending coronary artery. The merged image (right) clearly shows accumulation of ^{19}F signal near the infarcted region and at the location of surgery where the thorax was opened. Bottom: Sections of ^{1}H images superimposed with the matching ^{19}F images (red) acquired 1, 3, and 4 days after surgery indicate a time-dependent infiltration of PFCs into injured areas of the heart and the adjacent region of the chest affected by thoracotomy.

Repetitive measurements from day 1 after ligation of the coronary artery reveal a time-dependent accumulation of PFCs within the infarcted region as shown in Figure 4 lower row. The end-diastolic ^{1}H images acquired 1, 2, and 4 days after induction of myocardial infarction show the progressive left ventricular dilatation as a consequence of the insult. Merging with the matching ^{19}F images (red) demonstrates the successive infiltration of PFC-loaded immune cells into the affected area of the heart and the region of the chest injured by surgery. Detected ^{19}F signals are restricted to the area near the infarcted region of the heart; at no time infiltrating PFCs are observed within the unimpaired septum. This suggests that not only is it possible to clearly detect specific areas of inflammation, but it is also feasible to assess the degree of the induced immune response.

Conclusions

The combined use of several MR techniques allows to gain a comprehensive picture of murine disease models and permit a thorough analysis of pathomechanisms relevant for the human setting. Due to the noninvasive nature of these investigations, repetitive measurements can serve to monitor the progression of heart diseases and to assess the success of suitable therapies. This will help to explore underlying causes of human cardiomyopathies and to further enable identification of novel therapeutic targets as well as development and verification of new investigational drugs.

References

[1] Vanhoutte L, Gerber BL, Gallez B, Po C, Magat J, Ballig and J-L, Feron O, Moniotte S. High field magnetic resonance imaging of rodents in cardiovascular research. *Basic Res Cardiol.* **2016**;111:46.

[2] Wiesmann F, Ruff J, Dienesch C, Leupold A, Rommel E, Haase A, Neubauer S. Cardiovascular phenotype characterization in mice by high resolution magnetic resonance imaging. *Magn Reson Mater Phy.* **2000**;11:10–15.

[3] Akki A, Gupta A, Weiss RG. Magnetic resonance imaging and spectroscopy of the murine cardiovascular system. *Am J Physiol Heart Circ Physiol.* **2013**;304:H633-648.

[4] Bakermans AJ, Abdurrachim D, Moonen RPM, Motaal AG, Prompers JJ, Strijkers GJ, Vandoorne K, Nicolay K. Small animal cardiovascular MR imaging and spectroscopy. *Prog Nucl Magn Reson Spectrosc.* **2015**;88–89:1–47.

[5] Flögel U, Gödecke A, Klotz L-O, Schrader J. Role of myoglobin in the antioxidant defense of the heart. *FASEB J.* **2004**;18:1156–1158.

[6] Flögel U, Jacoby C, Gödecke A, Schrader J. In vivo 2D mapping of impaired murine cardiac energetics in NO-induced heart failure. *Magn Reson Med.* **2007**;57:50–58.

[7] Jacoby C, Flögel U. MR for the investigation of murine vasculature. *Methods Mol Biol.* **2011**;771:439–456.

[8] Jacoby C, Böring YC, Beck A, Zernecke A, Aurich V, Weber C, Schrader J, Flögel U. Dynamic changes in murine vessel geometry assessed by high-resolution magnetic resonance angiography: a 9.4T study. *J Magn Reson Imaging.* **2008**;28:637–645.

[9] Flögel U, Ahrens E, editors. Fluorine Magnetic Resonance Imaging. Singapore: Pan Stanford Publishing; **2017**.

[10] Holland GN, Bottomley PA, Hinshaw WS. ^{19}F magnetic resonance imaging. *J Magn Reson.* **1977**;28:133–136.

[11] Bulte JWM. Hot spot MRI emerges from the background. *Nat Biotechnol.* **2005**;23:945–946.

[12] Haberkorn SM, Jacoby C, Ding Z, Keul P, Bönner F, Polzin A, Levkau B, Schrader J, Kelm M, Flögel U. Cardiovascular magnetic resonance relaxometry predicts regional functional outcome after experimental myocardial infarction. *Circ Cardiovasc Imaging.* **2017**;10:e006025.

[13] Hendgen-Cotta UB, Esfeld S, Coman C, Ahrends R, Klein-Hitpass L, Flögel U, Rassaf T, Totzeck M. A novel physiological role for cardiac myoglobin in lipid metabolism. *Sci Rep.* **2017**;7:srep43219.

[14] Böring YC, Flögel U, Jacoby C, Heil M, Schaper W, Schrader J. Lack of ecto-5′-nucleotidase (CD73) promotes arteriogenesis. *Cardiovasc Res.* **2013**;97:88–96.

[15] Flögel U, Ding Z, Hardung H, Jander S, Reichmann G, Jacoby C, Schubert R, Schrader J. In vivo monitoring of inflammation after cardiac and cerebral ischemia by fluorine magnetic resonance imaging. *Circulation.* **2008**;118:140–148.

[16] Ebner B, Behm P, Jacoby C, Burghoff S, French BA, Schrader J, Flögel U. Early assessment of pulmonary inflammation by ^{19}F MRI in vivo. *Circ Cardiovasc Imaging.* **2010**;3:202–210.

[17] Jelenik T, Flögel U, Álvarez-Hernández E, Scheiber D, Zweck E, Ding Z, Rothe M, Mastrototaro L, Kohlhaas V, Kotzka J, Knebel B, Müller-Wieland D, Moellendorf S, Gödecke A, Kelm M, Westenfeld R, Roden M, Szendroedi J. Insulin resistance and vulnerability to cardiac ischemia. *Diabetes.* **2018**;67:2695–2702.

[18] Scholz D, Ziegelhoeffer T, Helisch A, Wagner S, Friedrich C, Podzuweit T, Schaper W. Contribution of arteriogenesis and angiogenesis to postocclusive hindlimb perfusion in mice. *J Mol Cell Cardiol.* **2002**;34:775–787.

[19] Temme S, Bönner F, Schrader J, Flögel U. ^{19}F magnetic resonance imaging of endogenous macrophages in inflammation. *Wiley Interdiscip Rev Nanomed Nanobiotechnol.* **2012**;4:329–343.

www.bruker.com ● **Bruker BioSpin**

info@bruker.com